



**HAL**  
open science

## Modelling honeybee visual guidance in a 3-D environment

G. Portelli, Julien Serres, F. Ruffier, N. Franceschini

► **To cite this version:**

G. Portelli, Julien Serres, F. Ruffier, N. Franceschini. Modelling honeybee visual guidance in a 3-D environment. *Journal of Physiology - Paris*, 2010, 104 (1-2), pp.27-39. 10.1016/j.jphysparis.2009.11.011 . hal-02010550

**HAL Id: hal-02010550**

**<https://amu.hal.science/hal-02010550>**

Submitted on 7 Feb 2019

**HAL** is a multi-disciplinary open access archive for the deposit and dissemination of scientific research documents, whether they are published or not. The documents may come from teaching and research institutions in France or abroad, or from public or private research centers.

L'archive ouverte pluridisciplinaire **HAL**, est destinée au dépôt et à la diffusion de documents scientifiques de niveau recherche, publiés ou non, émanant des établissements d'enseignement et de recherche français ou étrangers, des laboratoires publics ou privés.

# Modelling honeybee visual guidance in a 3-D environment

Portelli G., Serres J., Ruffier F., and Franceschini N.

*The Institute of Movement Sciences, UMR6233 CNRS - Aix-Marseille Uni., CP938, 163 ave. Luminy, 13288 Marseille Cedex 09, France*

---

## Abstract

In view of the behavioral findings published on bees during the last two decades, it was proposed to decipher the principles underlying bees' autopilot system, focusing in particular on these insects' use of the optic flow (OF). Based on computer-simulated experiments, we developed a vision-based autopilot that enables a "simulated bee" to travel along a tunnel, controlling both its speed and its clearance from the right wall, left wall, ground, and roof. The flying agent thus equipped enjoys three translational degrees of freedom on the surge ( $x$ ), sway ( $y$ ), and heave ( $z$ ) axes, which are uncoupled. This visuo-motor control system, which is called ALIS (AutopiLot using an Insect based vision System), is a *dual OF regulator* consisting of two interdependent feedback loops, each of which has its own OF set-point. The experiments presented here showed that the simulated bee was able to navigate safely along a straight or tapered tunnel and to react appropriately to any untoward OF perturbations, such as those resulting from the occasional lack of texture on one wall or the tapering of the tunnel. The minimalistic visual system used here (involving only eight pixels) suffices to jointly control both the clearance from the four walls and the forward speed without

having to measure any speeds or distances. The OF sensors and the simple visuo-motor control system we have developed account well for the results of ethological studies performed on honeybees flying freely along straight and tapered corridors.

*Key words:* Optic Flow (OF), computational neurosciences, honeybee, speed control, biomimetics, obstacle avoidance.

---

## 1. INTRODUCTION

Winged insects are able to navigate in unfamiliar environments, using the optic flow (OF) (Gibson, 1950) generated by their own motion (Horridge, 1987). Insects make use of the OF to avoid lateral obstacles (Srinivasan et al., 1991; Serres et al., 2008b), control their speed (Preiss, 1987; Baird et al., 2005, 2006) and height (Baird et al., 2006; Franceschini et al., 2007), cruise and land (Srinivasan et al., 1996, 2000; Franceschini et al., 2007). Behavioral studies on flying insects have inspired several researchers to develop visually guided mobile robots (Pichon et al., 1989; Franceschini et al., 1992; Coombs and Roberts, 1992; Duchon and Warren, 1994; Santos-Victor et al., 1995; Weber et al., 1997; Lewis, 1997; Netter and Franceschini, 2002; Ruffier and Franceschini, 2003; Humbert et al., 2007; Beyeler et al., 2007).

The LORA III autopilot we previously developed was based on a pair of lateral OF regulators steering a *fully actuated* hovercraft, in which the surge and sway dynamics were uncoupled (Serres et al., 2008a). The LORA III autopilot was found to account for the behaviors such as *centering* and *speed control* observed in bees flying along stationary and nonstationary corridors (Srinivasan et al., 1991) as well as tapered corridors (Srinivasan et al., 1996). LORA III also accounted for the novel findings on *wall-following* (Serres et al., 2008b), which the previous hypothesis (“optic flow balance” hypothesis) could not explain.

In the ALIS autopilot described here, the LORA III autopilot principle is extended to include the vertical plane. The problem consisted here of developing a functional scheme for a joint speed control and obstacle avoidance system that would take not only *lateral* obstacles but also *ventral* obstacles

26 (Baird et al., 2006; Franceschini et al., 2007), and *dorsal* obstacles (Vickers  
27 and Baker, 1994) into account. The ALIS autopilot we designed was used  
28 to test a simulated honeybee, in which all the translational degrees of free-  
29 dom (DOF) (surge, sway, and heave) were uncoupled (Ellington, 1984). In  
30 our simulations, the flying agent was endowed with the following novel flight  
31 features:

- 32 • use of 2-D model for photoreceptor sensitivity,
- 33 • use of the walls, ground, and roof, which were all textured with *natural*  
34 scenes,
- 35 • use of a new linearized model for flying bees' locomotion.
- 36 • use of an optic flow regulator based on both the *lateral* and the *vertical*  
37 OFs.

38 The ALIS autopilot regulates the OF thanks to the positioning and for-  
39 ward control systems with which it is equipped, according to the following  
40 principles:

41 (i) the first OF regulator adjusts the bee's forward speed so as to keep  
42 whichever sum of the two opposite OFs (i.e., left/right or ventral/dorsal) is  
43 maximum equal to a *forward OF set-point*. The outcome is that the bee's  
44 forward speed becomes proportional to the smallest dimension (either the  
45 width or the height) of the flight tunnel. The forward speed attained will be  
46 such that the OF generated equals the value of the *forward OF set-point*.

47 (ii) the second OF regulator adjusts the bee's lateral or vertical position  
48 so as to keep whichever OF is maximum (among the four OFs : left, right,

49 ventral, and dorsal) equal to the *positioning OF set-point*. The outcome is  
50 that the clearance from the nearest tunnel surface (the walls, ground, or roof)  
51 becomes proportional to the bee’s current forward speed, as defined in (i).  
52 The clearance from the nearest tunnel will be such that the OF generated  
53 equals to the *positioning OF set-point*.

54 The ALIS autopilot enables the agent to perform obstacle avoidance by  
55 performing maneuvers involving only translational DOFs, unlike the obsta-  
56 cle avoidance schemes based on body saccades that involve rotational DOFs  
57 (Lewis, 1997; Schilstra and van Hateren, 1999; Tammero and Dickinson, 2002;  
58 Beyeler et al., 2007). The ALIS autopilot operates without relying on any  
59 speed or distance measurements. It also differs fundamentally from previ-  
60 ous “insect-like” navigation systems based on *speed* or *distance regulation*  
61 (Dickson et al., 2006).

62 In section 2, the dynamical model for the simulated bee is described in  
63 terms of its three translational DOFs. In section 3, the simulation set-up  
64 used to test the ALIS autopilot on board the simulated bee is described.  
65 Section 4 describes the ALIS autopilot in detail. Section 5 gives the results  
66 of computer-simulated experiments carried out on the simulated bee, which  
67 is able to perform various tasks such as takeoff, straight and tapered tunnel-  
68 following, and to react appropriately to any local lack of lateral or dorsal  
69 OF.

## 70 2. DYNAMICAL MODEL FOR BEES’ FLIGHT

71 Here we focus on the visuomotor feedback loops that may explain how  
72 a flying insect controls its speed and avoids obstacles. A linearized model

73 for the bee’s dynamics is proposed in terms of the three *translational* DOFs  
74 (surge, sway, and heave dynamics). Linearization was justified here by the  
75 limited range of speeds (0-2 m/sec) possible. The value of the three *rota-*  
76 *tional* DOFs was kept at zero because bees are known to fly straight to their  
77 nectar source (von Frisch, 1948; Riley et al., 2003). In our experiments, the  
78 simulated insect was not subjected to any wind disturbances: the ground-  
79 speed was therefore taken to be equal to the airspeed. The bee’s dynamic  
80 performances in the three translational DOFs will be described in detail be-  
81 low.

82 (FIGURE 1 about here)

### 83 2.1. Bees’ Surge dynamics

84 Experiments on fruitflies (David, 1978) and honeybees (Nachtigall et al.,  
85 1971; Esch et al., 1975) have shown that flying insects gain forward speed  
86 by pitching their mean flight-force vector  $\vec{F}$  forward at a small angle  $\theta_{pitch}$   
87 ( $\leq 20$  deg) with respect to the vertical (Fig. 1A, B). By slightly changing the  
88 wing stroke plane pitch angle  $\theta_{pitch}$ , the insect generates a forward Thrust  $T$ ,  
89 which hardly affects the vertical Lift  $L$  (Ellington, 1984). In bees, the mean  
90 flight-force vector orientation differs from the body orientation, forming a  
91 fixed angle (Nachtigall et al., 1971; Ellington, 1984).

### 92 2.2. Bees’ Sway dynamics

93 In flying hymenopterans, sideslip motion results from roll changes (Elling-  
94 ton, 1984; Zeil et al., 2008). The wing stroke plane roll angle  $\theta_{roll}$  therefore  
95 drives the Sideways thrust  $S$  (Fig. 1A, C).

96 *2.3. Bees' Heave dynamics*

97 The mean flight-force vector  $\vec{F}$  (Eq. 1) resulting from the wing stroke am-  
 98 plitude  $\Phi$  (Dillon and Dudley, 2004; Altshuler et al., 2005) can be expressed  
 99 in terms of forward Thrust  $T$ , Side thrust  $S$ , and vertical Lift  $L$ .

$$\vec{F} = \begin{Bmatrix} T \\ S \\ L \end{Bmatrix} = \begin{Bmatrix} F(\Phi) \cdot \sin \theta_{pitch} \cdot \cos \theta_{roll} \\ F(\Phi) \cdot \cos \theta_{pitch} \cdot \sin \theta_{roll} \\ F(\Phi) \cdot \cos \theta_{pitch} \cdot \cos \theta_{roll} \end{Bmatrix} \quad (1)$$

100 where  $F(\Phi)$  is the force generated by an amplitude  $\Phi$  of the wing stroke.  
 101 At small angles ( $\theta_{pitch}$  and  $\theta_{roll}$ ) angles,  $L$  is roughly equal to  $F$ . The wing  
 102 stroke amplitude  $\Phi$  therefore mainly drives the vertical lift  $L$ .

103 *2.4. Calculating the gain between the wing stroke amplitude and the lift*

104 The lift produced by a bee depends on both the density  $\rho$  of the air and  
 105 the wing stroke amplitude  $\Phi$  (Dudley, 1995). In order to determine the gain  
 106  $K_{wing}$  between the wing stroke amplitude  $\Phi$  and the lift  $L$ , we used the results  
 107 of experiments on *hovering bees* that were carried out in media with different  
 108 densities. Hovering bees were filmed in normal air ( $\rho_{Air} = 1,21 \text{ kg/m}^3$ ) and  
 109 in heliox ( $\rho_{Heliox} = 0,41 \text{ kg/m}^3$ ) (Altshuler et al., 2005). In the low density  
 110 heliox, bees were found to increase their wing stroke amplitude  $\Phi$  from 90 deg  
 111 to 130 deg, while keeping their wingbeat frequency constant. In these two  
 112 hovering situations ( $\theta_{pitch} = \theta_{roll} = 0^\circ$ ), the lift  $L$  is equal to the weight:

$$L_{Heliox}(\Phi = 130 \text{ deg}) = L_{Air}(\Phi = 90 \text{ deg}) = m \cdot g \cong 1 \text{ mN}$$

113 In a steady state analysis, the lift is proportional to the density at a given  
 114 stroke amplitude  $\Phi = 130 \text{ deg}$  (Ellington, 1984; Sane and Dickinson, 2002):



$$L_{Air}(\Phi = 130 \text{ deg})/\rho_{Air} = L_{Heliox}(\Phi = 130 \text{ deg})/\rho_{Heliox}$$

115 We therefore calculated  $L_{Air}(\Phi = 130 \text{ deg}) \cong 3 \text{ mN}$ , and obtained the  
 116 mean sensitivity of the lift production to the wing stroke amplitude,  $K_{wing} =$   
 117  $\partial L_{Air}/\partial \Phi = 50 \mu\text{N}/\text{deg}$  in hovering bees ( $\Phi_{Hover} = 90 \text{ deg}$ ).

### 118 2.5. The Linearized Flying Bee model

119 At small pitch levels  $|\theta_{pitch}| \leq 20 \text{ deg}$  and roll  $|\theta_{roll}| \leq 20 \text{ deg}$  angles, each  
 120 component of the mean flight-force vector  $\vec{F}$  can be linearized on the surge,  
 121 sway, and heave axes (Eq. 2) as a function of the pitch angle  $\theta_{pitch}$ , the roll  
 122 angle  $\theta_{roll}$ , and the wing stroke amplitude  $\Phi = \Phi_{Hover} + \Delta\Phi$ , respectively:

$$\vec{F} = \begin{Bmatrix} T \\ S \\ L \end{Bmatrix} = \begin{Bmatrix} m \cdot g \cdot \theta_{pitch} \\ m \cdot g \cdot \theta_{roll} \\ K_{wing} \cdot (\Phi_{Hover} + \Delta\Phi) \end{Bmatrix} \quad \text{with } K_{wing} \cdot \Phi_{Hover} = m \cdot g \quad (2)$$

123 The following linearized system of equations was referred to the bee's  
 124 center of gravity as follows:

$$m \cdot d\vec{V}/dt + Z \cdot \vec{V} = \vec{F} + m \cdot \vec{g} \quad (3)$$

125 where  $\vec{V}$  is the mean speed vector,  $\vec{F}$  is the mean flight force vector,  $\vec{g}$  is  
 126 the gravity constant,  $m = 100 \text{ mg}$  (the bee's mass), and  $Z$  is the translational

127 viscous friction matrix  $Z = \begin{bmatrix} \zeta & 0 & 0 \\ 0 & \zeta & 0 \\ 0 & 0 & \zeta \end{bmatrix}$ .

128 The time constant along a translational DOF can be defined by the ratio  
 129 between the mass and the translational viscous friction coefficient. To the  
 130 best of our knowledge, no data are available so far on the *sway* and *heave time*  
 131 *constants* in the case of freely flying honeybees but these values are likely to  
 132 be of the same order as the *surge time constant*. The *bee's surge time constant*  
 133  $\tau = m/\zeta = 0.22$  sec can be estimated from bees' landing data (Srinivasan  
 134 et al., 2000) and from bees OF based autopilot system (Franceschini et al.,  
 135 2007). In what follows, *bee sway* and *bee heave time constants* are assumed  
 136 to be equal to the *bee surge time constant*.

137 Equation 3 can be written as follows:

$$\begin{cases} \tau \cdot dV_x/dt + V_x = (m \cdot g)/\zeta \cdot \theta_{pitch} \\ \tau \cdot dV_y/dt + V_y = (m \cdot g)/\zeta \cdot \theta_{roll} \\ \tau \cdot dV_z/dt + V_z = (K_{wing}/\zeta) \cdot \Delta\Phi \end{cases} \quad (4)$$

138 The sensitivity  $K_{surge}$  of the forward speed  $V_x$  to the pitch angle  $\theta_{pitch}$   
 139 can be determined from **figure 2b** in Esch et al. (1975) and estimated as  
 140 follows:

$$K_{surge} = |\partial V_x / \partial \theta_{pitch}| = 0.10 \text{ m} \cdot \text{sec}^{-1} \cdot \text{deg}^{-1}$$

141  $K_{sway}$  is assumed to have a similar value:  $K_{sway} = K_{surge}$

142 The Laplace transfer functions giving the bee's surge dynamics  $G_{V_x}(s)$ ,  
 143 sway dynamics  $G_{V_y}(s)$ , and heave dynamics  $G_{V_z}(s)$  can therefore be written  
 144 as follows:

$$\left\{ \begin{array}{l} G_{V_x}(s) = \frac{V_x(s)}{\theta_{pitch}(s)} = \frac{K_{surge}}{1 + \tau_{surge} \cdot s} = \frac{0.10}{1 + 0.22 \cdot s} \quad (5a) \\ G_{V_y}(s) = \frac{V_y(s)}{\theta_{roll}(s)} = \frac{K_{sway}}{1 + \tau_{sway} \cdot s} = \frac{0.10}{1 + 0.22 \cdot s} \quad (5b) \\ G_{V_z}(s) = \frac{V_z(s)}{\Delta\Phi(s)} = \frac{K_{wing}/\zeta_z}{1 + \tau_{heave} \cdot s} = \frac{0.11}{1 + 0.22 \cdot s} \quad (5c) \end{array} \right.$$

145 The pitch angle was limited here to  $|\theta_{pitch}| \leq 20$  deg so as to keep the  
 146 maximum forward speed range to  $V_{xMax} = 2$  m/sec, and the roll angle was  
 147 limited to  $|\theta_{roll}| \leq 5$  deg so as to keep the maximum lateral speed range  
 148 to  $V_{yMax} = 0.5$  m/sec. Bees are thought to reach the maximum stroke  
 149 amplitude  $\Phi_{max} = 140$  deg and the minimum stroke amplitude  $\Phi_{min} =$   
 150  $70$  deg (Dudley, 2000; Dillon and Dudley, 2004). The maximum ascent speed  
 151  $V_{zUpMax}$  and the maximum descent speed  $V_{zDownMax}$  on the heave-axis are  
 152 therefore:

$$\left\{ \begin{array}{l} V_{zUpMax} = \quad (6a) \\ (K_{wing}/\zeta_z) \cdot (\Phi_{max} - \Phi_{Hover}) = 5.5 \text{ m/sec} \\ V_{zDownMax} = \quad (6b) \\ (K_{wing}/\zeta_z) \cdot (\Phi_{Hover} - \Phi_{min}) = -2.2 \text{ m/sec} \end{array} \right.$$

153 The bees' ascent speed, was calculated from **figure 7b** in Srinivasan et  
 154 al. (2000) and found to be equal to  $\approx 2$  m/sec. The bees' descent speed  
 155 measured during landing manoeuvres reaches a value of 2 m/sec (**figure 6d**  
 156 in Srinivasan et al. (2000)): this value is quite similar to our own predictions  
 157 (Eq. 6). In order to limit the vertical speed ( $|V_z| = 2$  m/sec), we set the  
 158 maximum stroke amplitude at  $|\Delta\Phi| \leq 18$  deg.

### 159 3. SIMULATION SET-UP

#### 160 3.1. Simulated 3-D environment

161 The simulated 3-D visual environment consisted of a straight or tapered  
162 flight tunnel (6 meters long, 1 meter wide, and 1 meter high), the four walls  
163 of which were lined with high resolution photographs of natural panoramic  
164 scenes (Brinkworth and O’Carroll, 2007). These images were converted into  
165 256 grayscale levels and resized keeping the original size ratios. One image  
166 pixel corresponded to one millimeter of the simulated environment (Fig. 2).  
167 The four natural grayscale images are shown in Fig. 2: right wall (Fig. 2A),  
168 left wall (Fig. 2B), roof (Fig. 2C), and ground (Fig. 2D).

169 (FIGURE 2 about here)

#### 170 3.2. Optic flow generated by the bee’s own motion

171 The simulated bee was assumed to be flying at a speed vector  $\vec{V}$  along the  
172 flight tunnel covered with natural-scene textures (Fig. 2). It has been shown  
173 that hymenopterans stabilize their gaze by compensating for any body rota-  
174 tions (Zeil et al., 2008), in much the same way as the blowfly does (Schilstra  
175 and van Hateren, 1999). The bee’s head orientation was therefore assumed to  
176 be locked to the X-axis of the tunnel. Since any rotation is compensated for,  
177 each OF sensor will receive a purely translational OF, which is the angular  
178 velocity of the environmental features detected by the lateral (diametrically  
179 opposed) and vertical (also diametrically opposed) OF sensors (Fig. 3).

180 The translational OF can be defined simply as the forward speed-to-  
181 distance ratio (expressed in rad/sec) in line with (7).

$$\omega_i = V_x/D_i, \quad \text{with } i \in \{Right, Left, Vtrl, Drsl\} \quad (7)$$

182 where  $V_x$  is the bee’s forward speed,  $D_{Right}$ ,  $D_{Left}$  are the distances to the  
 183 side (right and left) walls, and  $D_{Vtrl}$ ,  $D_{Drsl}$  are the distances to the ground  
 184 (ventral eye) and to the roof (dorsal eye) (Fig. 3). Each OF sensor receives  
 185 its own OF, which can be a right OF ( $\omega_{Right}$ ), a left OF ( $\omega_{Left}$ ), a ventral OF  
 186 ( $\omega_{Vtrl}$ ), or a dorsal OF ( $\omega_{Drsl}$ ).

187 (FIGURE 3 about here)

### 188 3.3. *OF sensors on board the simulated bee*

189 Bees are endowed with two compound eyes, each of which is composed of  
 190 4500 ommatidia. The visual axes of two adjacent ommatidia are separated  
 191 by an interommatidial angle  $\Delta\varphi$ , which varies from one region of the eye to  
 192 another (Seidl and Kaiser, 1981). Each ommatidium is composed of a lens  
 193 and nine photoreceptor cells with identical receptive fields. Six of these cells  
 194 have a green spectral sensitivity (Wakakuwa et al., 2005) and are involved  
 195 in motion vision. These photoreceptor cells are connected to three succes-  
 196 sive visual optic lobes: the lamina, the medulla, and the lobula. Further  
 197 down the visual processing chain, descending neurons have been found to re-  
 198 spond to object velocity (Velocity-Tuned motion-sensitive neurons VT cells  
 199 in Ibbotson (2001)). VT neurons respond monotonically to front-to-back  
 200 translational movements, and therefore act like real *OF sensors*. Our sim-  
 201 ulated bee is equipped with only four OF sensors (two lateral, one ventral,  
 202 and one dorsal sensor, Fig. 3A). Each of these sensors consists of only two  
 203 photoreceptors (two pixels) driving an Elementary Motion Detector (EMD).

204 The visual axes of the two photoreceptors are assumed to be separated by an  
205 angle  $\Delta\varphi = 4$  deg. Each photoreceptor’s angular sensitivity is assumed to be  
206 a Gaussoid function with an acceptance angle (angular width at half height)  
207  $\Delta\rho = 4$  deg, and a total field of view of  $10.4 \text{ deg} \times 10.4 \text{ deg}$ . The photorecep-  
208 tors’ output was computed at each time step (0.5 msec) by multiplying two  
209 matrixes:

- 210 • a matrix representing the visible local natural scene (Fig. 2),
- 211 • a matrix representing the insect-like photoreceptor Gaussoid sensitivity.

212 The “time-of-travel” scheme of the bio-inspired EMD developed by Frances-  
213 chini’s research group has been previously described in detail (Blanes, 1986;  
214 Pudas et al., 2007; Aubépart and Franceschini, 2007; Franceschini et al.,  
215 2009). The response of this OF sensor is a monotonic function of the angular  
216 velocity within a 10-fold range (from 40 deg/sec to 400 deg/sec) (Ruffier and  
217 Franceschini, 2005), resembling that of the Velocity-Tuned motion-sensitive  
218 descending neurons found to exist in honeybees(VT neurons: Ibbotson, 2001).

#### 219 4. THE ALIS AUTOPILOT

220 The simulated bee is controlled by an autopilot called ALIS (which stands  
221 for AutopiLot using an Insect-based vision System), which is reminiscent of  
222 both the OCTAVE autopilot for ground avoidance (Ruffier and Franceschini,  
223 2005) and the LORA III autopilot for speed control and lateral obstacle  
224 avoidance (Serres et al., 2008a) previously developed at our laboratory. The  
225 ALIS autopilot relies, however, on four OF measurements: right, left, ventral,  
226 and dorsal. We designed the ALIS autopilot assuming that speed control

227 and obstacle avoidance problems could be solved in a similar way in both the  
 228 horizontal and vertical planes. The ALIS autopilot consists of two visuomotor  
 229 feedback loops: the *speed control* loop (on the surge axis) and the *positioning*  
 230 *control* loop (on the sway and heave axes). These two loops work in parallel  
 231 and are *interdependent*. Each of them involves multiple processing stages  
 232 (Fig. 4), and each has its own OF set-point: the *forward OF set-point* and  
 233 the *positioning OF set-point*, respectively. In this dual control system, neither  
 234 the speed nor the distance from the tunnel surfaces (walls, ground, or roof)  
 235 need to be *measured*. The simulated bee will react to any changes in the OFs  
 236 by selectively adjusting the three orthogonal components  $V_x$ ,  $V_y$ , and  $V_z$  of  
 237 its speed vector  $\vec{V}$ .

(FIGURE 4 about here)

#### 239 4.1. Forward speed control and forward speed criterion

240 The *speed control* loop was designed to hold the maximum sum of the two  
 241 diametrically opposed OFs (measured in the horizontal and vertical planes)  
 242 constant and equal to a forward OF set-point  $\omega_{setFwd}$ . The ALIS autopilot  
 243 does so by adjusting the forward thrust  $T$  (that will determine the forward  
 244 speed  $V_x$ ). In other words, this regulation process consists in first determining  
 245 whether the sum of the OFs measured in the horizontal plane ( $\omega_{Right}^m + \omega_{Left}^m$ )  
 246 or the sum of those measured in the vertical plane ( $\omega_{Vtrl}^m + \omega_{Drsl}^m$ ), is the  
 247 larger of the two. The larger of the two sums is then compared with the  
 248 forward OF set-point  $\omega_{setFwd}$  (blue loop, Fig. 4). The forward OF set-point  
 249 was set at:  $\omega_{setFwd} = 4.57 \text{ V}$  (i.e., 540 deg/sec). This value was based on that  
 250 recorded in freely flying bees (Baird et al., 2005). The error signal  $\varepsilon_{Fwd}$  (the  
 251 input to the surge controller) is calculated as follows:

$$\varepsilon_{Fwd} = \omega_{setFwd} - \max[(\omega_{Rght}^m + \omega_{Left}^m), (\omega_{Vtrl}^m + \omega_{Drsl}^m)] \quad (8)$$

252 The surge controller was tuned using the same procedures as those previ-  
 253 ously described in the case of the LORA III autopilot (Serres et al., 2008a).

#### 254 4.2. Positioning control and positioning criterion

255 The *positioning control* loop is in charge of positioning the bee with  
 256 respect to either the side walls or the ground or the roof of the tunnel.  
 257 Whether this positioning involves motion on the sway or the heave axis  
 258 depends on whether the maximum OF measured is in the horizontal or  
 259 vertical plane. The regulation process adopted here is based on the max-  
 260 imum value of the four OFs measured ( $\max(\omega_{Rght}^m, \omega_{Left}^m, \omega_{Vtrl}^m, \omega_{Drsl}^m)$ ), the  
 261 red loop in Fig. 4), i.e., the value given by the nearest tunnel surface (walls,  
 262 ground, or roof). This OF regulator is designed to maintain whichever of  
 263 the four OFs measured is the larger equal to the positioning OF set-point  
 264  $\omega_{setPos}$ . The larger OF measured is compared with  $\omega_{setPos}$ , which was set  
 265 at:  $\omega_{setPos} = 2.4 \text{ V}$  (i.e., 315 deg/sec). This value was again based on that  
 266 recorded in freely flying bees (Baird et al., 2005). The error signal  $\varepsilon_{Pos}$  (the  
 267 input to the positioning controller) is calculated as follows:

$$\varepsilon_{Pos} = \omega_{setPos} - \max(\omega_{Rght}^m, \omega_{Left}^m, \omega_{Vtrl}^m, \omega_{Drsl}^m) \quad (9)$$

268 The positioning controller was tuned using the same procedures as those  
 269 previously described in the case of the LORA III autopilot (Serres et al.,  
 270 2008a).

271 (FIGURE 5about here)



272 The surface that will be followed (walls, ground or roof) is specified by  
273 a *Control direction Selector* (Fig. 4, 5). The positioning control signal  
274 is multiplied by a *direction factor* that corresponds to the *direction of the*  
275 *maximum OF* signal. Note that the sway and heave dynamics can be driven  
276 alternately, depending on whichever (lateral or vertical) OF is maximum at  
277 any given time. The input to the type of dynamics is *not* commanded is then  
278 set at zero (Fig. 5) (Side thrust = 0 or Vertical lift = 0). The simulated  
279 bee will react to any unexpected changes in the OFs measured by adjusting  
280 either its lateral speed  $V_y$  (and hence its lateral position) or its vertical speed  
281  $V_z$  (and hence its vertical position). The OF regulator will always react to  
282 the nearest of the four tunnel surfaces.

## 283 5. SIMULATION RESULTS

### 284 5.1. Automatic tunnel-following

285 In Fig. 6, the simulated environment is a straight tunnel 6 meters long,  
286 1 meter wide, and 1 meter high. Fig. 6A shows a perspective view. Walls,  
287 ground, and roof were lined with natural grayscale images (Fig. 2). The  
288 simulated bee enters the tunnel at the speed  $V_{x0} = 0.2\text{m/sec}$  and with the  
289 initial coordinates  $x_0 = 0.1\text{m}$ , and various couples of  $y_0$  and  $z_0$  (Fig. 6B).  
290 Fig. 6C shows the five trajectories in the vertical plane (x, z) and Fig. 6D  
291 in the horizontal plane (x, y), plotted every 500 msec. Each bar indicates  
292 the honeybee's body orientation, which is known to form a fixed angle with  
293 the orientation of the mean flight-force vector (Nachtigall et al., 1971; David,  
294 1978).

295 The simulated bee can be seen to have gradually increased both its height

296 of flight (Fig. 6C) and its right clearance (Fig. 6D) to 0.33 m, while the for-  
297 ward speed (Fig. 6E) increased automatically up to 2 m/sec (i.e., the maxi-  
298 mum speed allowed) whichever is the initial positions.

299 These results show that the ALIS autopilot caused the simulated bee to  
300 travel safely along the tunnel, while reaching a given forward speed and a  
301 given clearance from the walls.

302 (FIGURE 6 and FIGURE 7 about here)

### 303 5.2. *Effect of the local absence of contrast on one of the internal faces of the* 304 *tunnel*

305 Fig. 7 shows successful tests on the behavior of the simulated bee in the  
306 presence of “no contrast” zones on the left wall or the roof of the tunnel.  
307 These “no contrast” zones could be either a real aperture or a lack of texture  
308 (Fig. 7A). The simulated bee was made to enter the tunnel at speed  $V_{x0} =$   
309 0.2 m/sec with the initial coordinates  $x_0 = 0.1$  m,  $y_0 = 0.85$  m,  $z_0 = 0.85$  m  
310 (Fig. 7B). Fig. 7C shows the trajectory in the vertical plane (x, z) and Fig. 7D  
311 in the horizontal plane (x, y), plotted every 500 msec.

312 As can be seen from Fig. 7, the simulated bee was not greatly disturbed  
313 by either the 2-meter long aperture encountered on its left-hand side (at the  
314 beginning of the tunnel) or a similar aperture entering its dorsal field of view  
315 (at the end of the tunnel).

316 The positioning criterion (Fig. 7F) could select either the left or dor-  
317 sal EMD output ( $\omega_{Left}^m$  or  $\omega_{Drsl}^m$ ) when there were no lateral or vertical OF  
318 outputs because of the presence of “no contrast” zones (from X= 0.5 m to  
319 X= 2.5 m and from X= 3.5 m to X= 5.5 m). The positioning criterion caused

320 the simulated bee to keep a dorsal clearance  $D_{DrsL} = 0.35$  m (Fig. 7C) and a  
321 left clearance  $D_{Left} = 0.39$  m (Fig. 7D) throughout its journey.

322 The forward criterion (Fig. 7G) could select either the vertical or horizon-  
323 tal EMD output when there were no lateral or vertical OF outputs because  
324 of the “no contrast” zones encountered (from  $X = 0.5$  m to  $X = 2.5$  m and  
325 from  $X = 3.5$  m to  $X = 5.5$  m). This criterion caused the simulated bee to  
326 maintain a relatively constant speed  $V_x = 1.85$  m/sec throughout its journey  
327 (Fig. 7E).

328 These results show that the ALIS autopilot enabled the simulated bee to  
329 travel safely along the tunnel without being greatly disturbed by the presence  
330 of a lateral or dorsal “no contrast” zone.

### 331 5.3. Automatic terrain-following

332 Fig. 8 shows successful tests on the behaviour of the simulated bee on a  
333 sloping terrain (slope angle 7,deg). As this sloping zone gradually affected  
334 the relative distance from the bee to the ground  $D_{Vtrl}$ , it acted like an OF  
335 perturbation (Fig. 8A). The simulated bee was made to enter the tunnel  
336 at the speed  $V_{x0} = 0.2$  m/sec with the initial coordinates  $x_0 = 0.1$  m,  $y_0 =$   
337  $0.85$  m,  $z_0 = 0.15$  m (Fig. 8B). Fig. 8C shows the trajectory in the vertical  
338 plane ( $x, z$ ) and Fig. 8D in the horizontal plane ( $x, y$ ), plotted every 500 msec.

339 (FIGURE 8 about here)

340 As can be seen from Fig. 8, the simulated bee was not greatly disturbed  
341 by the ramp-like slope occurring below its flight path.

342 The positioning criterion (Fig. 8F) could select either the ventral or left  
343 EMD output ( $\omega_{Vtlr}^m$  and  $\omega_{Left}^m$ ). This automatic choice caused the simu-

344 lated bee to maintain both a ventral clearance and a left clearance (Fig. 8D)  
345 throughout its journey.

346 The forward criterion can be seen to have mostly opted for vertical EMD  
347 outputs ( $\omega_{Vtlr}^m + \omega_{Drsl}^m$ , Fig. 8G) because the ventral slope made the vertical  
348 section of the tunnel smaller than its horizontal section. This criterion caused  
349 the simulated bee to maintain a relatively constant speed  $V_x = 1.45$  m/sec  
350 throughout its journey (Fig. 8E).

351 These results show that the ALIS autopilot made the simulated bee travel  
352 along the tunnel without being greatly disturbed by the sloping ground en-  
353 countered.

#### 354 5.4. Automatic speed control in horizontally and/or vertically tapered tunnels

355 The simulated tunnels used here were 6-meter long, 1-meter high tapered  
356 tunnels with a 1-meter wide entrance and a 0.25-meter constriction halfway  
357 along the tunnel. This constriction could occur in either the horizontal plane  
358 (Fig. 9A) the vertical plane (Fig. 10A), or both planes together (Fig. 11A).  
359 These tunnels were designed to test the ability of the ALIS autopilot to  
360 overcome several strong OF disturbances at the same time.

361 (FIGURE 9 and FIGURE 10 about here)

362 As shown in Fig. 9, the simulated bee was made to enter a tunnel with a  
363 midway constriction in the *horizontal* plane, at the speed  $V_{x0} = 0.2$  m/sec and  
364 with the initial coordinates  $x_0 = 0.1$  m,  $y_0 = 0.85$  m,  $z_0 = 0.15$  m (Fig. 9B).  
365 Fig. 9C shows the trajectory in the vertical plane (x, z) and Fig. 9D in the  
366 horizontal plane (x, y), plotted every 500 msec.

367 The simulated bee followed the left wall of the tapered tunnel, simply  
 368 because its starting point was close to that wall. The positioning criterion  
 369 (Fig. 9F) selected the left EMD output ( $\omega_{left}^m$ ), which remained approximately  
 370 equal to the *positioning OF set-point* throughout the journey (Fig. 9F). The  
 371 simulated bee kept a safe left clearance throughout its journey. The simulated  
 372 bee automatically slowed down as it approached the narrowest section of the  
 373 tapered tunnel, and accelerated again when the tunnel widened out beyond  
 374 that point (Fig. 9E). Since the tunnel narrowed only in the horizontal plane,  
 375 the OF in the vertical plane was of little relevance to the speed control part  
 376 of the ALIS autopilot. The forward speed depended mostly on the OF in  
 377 the horizontal plane ( $\omega_{Left}^m + \omega_{Right}^m$ , Fig. 9G) because the horizontal section  
 378 of the tunnel was smaller than its vertical section.

379 The ALIS autopilot made the simulated bee travel safely along the “*hor-*  
 380 *izontal*” tapered tunnel (tapering angle 7 deg) without being greatly per-  
 381 turbed by the major OF disturbance concomitantly detected by both its left  
 382 and right OF sensors.

383 As shown in Fig. 10, the simulated bee was then made to enter a tun-  
 384 nel with a midway constriction in the vertical plane, at the speed  $V_{x0} =$   
 385 0.2 m/sec, with the initial coordinates  $x_0 = 0.1$  m,  $y_0 = 0.85$  m,  $z_0 = 0.15$  m  
 386 (Fig. 10B). Fig. 10C shows the trajectory in the vertical plane (x, z) and  
 387 Fig. 10D in the horizontal plane (x, y), plotted every 500 msec. In this case,  
 388 the simulated bee followed both the ground and the left wall of the tapered  
 389 tunnel, simply because its starting point was near to the ground and the  
 390 left wall. The positioning criterion could select either the ventral or left OF  
 391 measured ( $\omega_{Vtlr}^m$  and  $\omega_{Left}^m$ ), which remained approximately equal to the *po-*

392 *sitioning OF set-point* throughout the journey (Fig. 10F). The simulated bee  
393 kept a safe ventral and left clearance throughout its journey.

394 The simulated bee automatically slowed down as it approached the nar-  
395 rowest section of the tapered tunnel, and accelerated again when the tunnel  
396 widened out beyond that point (Fig. 10E). As the tunnel narrowed only in  
397 the vertical plane, the OF in the horizontal plane was of little relevance to  
398 the speed control part of the ALIS autopilot. The forward speed depended  
399 mostly on the OF in the vertical plane ( $\omega_{vtrl}^m + \omega_{Drsl}^m$ , Fig. 10G) because the  
400 vertical section of the tunnel was smaller than its horizontal section.

401 The ALIS autopilot made the simulated bee travel along the vertically  
402 tapered tunnel (tapering angle 7 deg) without being greatly perturbed by the  
403 major OF disturbance concomitantly detected by both its ventral and dorsal  
404 OF sensors.

405 (FIGURE 11 about here)

406 As shown in Fig. 11, the simulated bee was then made to enter the tunnel  
407 with midway constrictions in both the horizontal and vertical planes. The bee  
408 entered at the speed  $V_{x0} = 0.2$  m/sec with the initial coordinates  $x_0 = 0.1$  m,  
409  $y_0 = 0.85$  m,  $z_0 = 0.15$  m (Fig. 11B). Fig. 11C shows the trajectory in the  
410 vertical plane (x, z) and Fig. 11D in the horizontal plane (x, y), plotted every  
411 500 msec. The simulated bee followed both the ground and the left wall of  
412 the tapered tunnel, simply because its starting point was near the ground  
413 and the left wall. The positioning criterion could select either the ventral or  
414 the left OF measured ( $\omega_{Vtrl}^m$  and  $\omega_{Left}^m$ ), which remained approximately equal  
415 to the *positioning OF set-point* throughout the trajectory (Fig. 11F). The  
416 simulated bee kept a safe ventral and left clearance throughout its journey.

417 The simulated bee automatically slowed down as it approached the nar-  
418 rowest section of the tapered tunnel and accelerated again when the tunnel  
419 widened out beyond this point (Fig. 11E). As the tunnel narrowed in both the  
420 horizontal and vertical planes, the OFs in the horizontal and vertical planes  
421 were both equally relevant to the speed control part of the ALIS autopilot.  
422 The forward speed depended on the OFs in both the horizontal and vertical  
423 planes ( $\omega_{Right}^m + \omega_{Left}^m$  and  $\omega_{Vtlr}^m + \omega_{Drsl}^m$ , Fig. 11G) because the horizontal and  
424 the vertical sections of the tunnel both varied to an equal extent.

425 The ALIS autopilot made the simulated bee cross the “horizontal and  
426 vertical” tapered tunnel (tapering angle 7 deg in both planes) without being  
427 greatly perturbed by a major overall OF disturbance concomitantly affecting  
428 its lateral, ventral, and dorsal OF sensors.

429 All in all, these results show that the ALIS autopilot made the simulated  
430 bee:

- 431 • adopt a cruise speed that will automatically adjust to whichever section  
432 (horizontal or vertical) produces the largest optic flow, and
- 433 • adopt a clearance from one of the tunnel surfaces (the ground or the  
434 roof or one wall) that will be proportional to the animal’s ground speed,  
435 thus automatically generating both *terrain-following* and *wall-following*  
436 behavior.

## 437 6. CONCLUSIONS

438 Here we have presented an OF-based 3D autopilot called ALIS. The re-  
439 sults of the computer simulations described above show that a simulated bee

440 equipped with the ALIS autopilot can navigate safely under purely visual  
441 control along a straight tunnel (Fig. 6), occurs even when part of the wall or  
442 the roof is devoid of texture (Fig. 7) and when the tunnel narrows or expands,  
443 in either the horizontal or vertical plane (Fig. 8A, 9A, 10A), or in both planes  
444 (Fig. 11A). Here we have not investigated dynamical disturbances such as  
445 wind perturbations but tested ALIS’s robustness to strong OF perturbations.  
446 Absence of contrast on one side (as Fig. 7) and tapered tunnels (Fig. 9- 11)  
447 are considered by the ALIS control system (Fig. 4) as strong perturbations.  
448 The autopilot manages to cope with these major perturbations, allowing the  
449 simulated bee to fly safely in these tunnels.

450 These feats can all be achieved with a really minimalistic visual system  
451 consisting of only eight pixels forming four EMDs (two EMDs in the hor-  
452 izontal plane and two in the vertical plane). The ALIS autopilot enables  
453 the agent to avoid obstacles by performing maneuvers involving only trans-  
454 lational DOFs (along  $x$ ,  $y$ ,  $z$ ). The key to the performances of the ALIS  
455 autopilot is a pair of *OF regulators* designed to hold the perceived OF con-  
456 stant by adjusting the forward, side, and vertical thrusts. More specifically,  
457 these two *OF regulators* operate as follows:

458 (i) The first *OF regulator* adjusts the bee’s forward speed so as to keep  
459 *whichever sum* of the two opposite OFs (i.e., left+right or ventral+dorsal)  
460 is maximum equal to a *forward OF set-point*. The outcome is that the bee’s  
461 forward speed becomes proportional to the smallest dimension (width or  
462 height, or both) of the corridor (Fig. 9E, 10E, 11E). Further simulations  
463 showed (data not shown) that this occurs regardless of the position of the  
464 bee’s starting point at the tunnel entrance. The forward speed attained by



465 the simulated bee depends also on the forward OF set-point  $\omega_{setFwd}$ .

466 (ii) The second *OF regulator* adjusts the bee’s lateral and vertical position  
467 so as to keep the *largest OF value* (from any of the four tunnel surfaces: walls,  
468 ground, or roof) equal to the *positioning OF set-point*. The outcome is that  
469 the clearance from the nearest wall (or ground or roof) becomes proportional  
470 to the bee’s forward speed as defined in (i). The clearance from the nearest  
471 tunnel surface depends on the positioning OF set-point  $\omega_{setPos}$ .

472 The main advantage of this visuomotor control system is that it operates  
473 efficiently without any needs for explicit speed or distance information, and  
474 hence without any needs for speed or range sensors. The emphasis here  
475 is on behavior rather than metrics: the simulated bee behaves appropriately  
476 although it is completely “unaware” of its ground speed and its distance from  
477 the walls, ground, and roof. The simulated bee navigates on the basis of two  
478 parameters alone: the forward OF set-point  $\omega_{setFwd}$  and the positioning OF  
479 set-point  $\omega_{setPos}$  (Fig. 4). The *explicit* ALIS control scheme presented here  
480 (Fig. 4) can be viewed as a working hypothesis and is very much in line with  
481 the ecological approach (Gibson, 1950), according to which an animal’s visual  
482 system is thought to drive the locomotor system directly, without requiring  
483 any “representation” of the environment (Franceschini et al., 1992; Duchon  
484 and Warren, 1994). The ALIS control scheme (Fig. 4) readily accounts for the  
485 behavior observed on real bees flying along a stationary corridor (Srinivasan  
486 et al., 1991; Serres et al., 2008b; Baird et al., 2006) or a tapered corridor  
487 (Srinivasan et al., 1996). It also accounts for the *wall-following* behavior  
488 observed in straight or tapered corridors (Serres et al., 2008b).

489 Real bees have 4500 ommatidia, per eye and obviously more than four

490 OF sensors. These large number of OF sensors therefore enable them to  
491 measure the OF in many directions and an elaborated autopilot could make  
492 them to avoid obstacles occurring in many directions. An OF regulator is  
493 little demanding in terms of its neural (or electronic) implementation since  
494 it requires only a few *linear* operations (such as adding, subtracting, and  
495 applying various filters) and *nonlinear* operations (such as minimum and  
496 maximum detection). The minimalist control scheme described in this paper  
497 could be implemented in a micro-controller running at 1kHz. In this way,  
498 the “computation time” could be up to 1 msec.

499 In terms of the potential applications of these findings, biomimetic solu-  
500 tions of the kind described here may pave the way for the design of computation-  
501 lean, lightweight visual guidance systems for autonomous aerial, underwater,  
502 and space vehicles.

#### 503 ACKNOWLEDGMENTS

504 We thank S. Viollet and L. Kerhuel for their fruitful comments and sug-  
505 gestions during this work, R. Brinkworth and D. O’Carroll (Adelaide Uni.,  
506 Australia) for kindly making their panoramic images available to us, and J.  
507 Blanc for improving the English manuscript. This work was supported partly  
508 by CNRS (Life Science; Information and Engineering Science and Technol-  
509 ogy), by the Aix-Marseille University, by the French Defense Agency (DGA,  
510 05 34 022), by the French Agency for Research (ANR, RETINAE project),  
511 and by the European Space Agency (ESA) under contract n° 08-6303b.

512 **References**

- 513 Altshuler, D.L., Dickson, W.B., Vance, J.T., Roberts, S.P., and Dickinson, M.H. (2005). Short-amplitude  
514 high-frequency wing strokes determine the aerodynamics of honeybee flight. PNAS. 102(50), 8213-  
515 18218.
- 516 Aubépart, F., and Franceschini, N. (2007). A bio-inspired optic flow sensor based on FPGA: application  
517 to micro-air-vehicles. J. of Microprocessors and Microsystems. 31(6), 408-419.
- 518 Baird, E., Srinivasan, M.V., Zhang, S., and Cowling, A. (2005). Visual control of flight speed in honeybees.  
519 J. Exp. Biol. 208, 3895-3905.
- 520 Baird, E., Srinivasan, M.V., Zhang, S., Lamont, R., and Cowling, A. (2006). Visual control of flight speed  
521 and height in honeybee. LNAI. 4095, 40-51.
- 522 Beyeler, A., Zufferey, J.-C., and Floreano, D. (2007). 3D vision-based navigation for indoor microflyers.  
523 Proc. IEEE Int. Conf. on Robotics and Automation. pp. 1336-1341.
- 524 Blanes, C. (1986). Appareil visuel élémentaire pour la navigation à vue d'un robot mobile autonome. MS  
525 in Neuroscience, Marseille, France: University of Aix-Marseille II.
- 526 Brinkworth, R.S.A., and O'Carroll, D.C. (2007). Biomimetic Motion Detection. Proc. of the Int. Conf. on  
527 Intelligent Sensors, Sensor Networks and Information Processing (ISSNIP). 3, 137-142.
- 528 Coombs, D., and Roberts, K. (1992). Bee-bot: using peripheral optical flow to avoid obstacle. SPIE:  
529 Intelligent robots and computer vision XI. 1825, 714-721.
- 530 David, C. (1978). The relationship between body angle and flight speed in free-flying *Drosophila*. *Physiol.*  
531 *Entomol.* 3, 191-195.
- 532 Dickson, W.B., Straw, A.D., Poelma, C., and Dickinson, M.H. (2006). An integrative model of insect flight  
533 control. Proc. of the 44th AIAA Aerospace Sciences Meeting and Exhibit. AIAA-2006-0034.
- 534 Dillon, M.E., and Dudley, R. (2004). Allometry of maximum vertical force production during hovering  
535 flight of neotropical orchid bees (*Apidae: Euglossini*). *J. Exp. Biol.* 207, 417-425.
- 536 Duchon, A.P., and Warren, W.H. (1994). Robot navigation from a Gibsonian viewpoint. Proc. Int. Conf.  
537 Syst. Man and Cyb. 2272-2277, San Antonio, Texas.
- 538 Dudley, R. (1995). Extraordinary flight performance of orchid bees (*apidae: euglossini*) hovering in heliox  
539 (80% He / 20% O<sup>2</sup>). *J. Exp. Biol.* 198, 1065-1070.

540 Dudley, R. (2000). *The biomechanics of insect flight: form, function, evolution*, (Princeton: Princeton  
541 University Press).

542 Ellington, C.P. (1984). The aerodynamics of hovering insect flight. III. Kinematics. *Phil. Trans. Roy. Soc.*  
543 *Lond. B.* 305, 41-78.

544 Esch, H., Nachtigall, W., and Kogge, S.N. (1975). Correlations between aerodynamic output, electrical  
545 activity in the indirect flight muscles and wing positions of bees flying in a servomechanically controlled  
546 flight tunnel. *J. Comp. Physiol.* 100, 147-159.

547 Franceschini, N., Pichon, J.M., and Blanes, C. (1992). From insect vision to robot vision. *Philos. Trans.*  
548 *R. Soc. Lond. B* 337, 283294.

549 Franceschini, N., Ruffier, F., and Serres, J. (2007). A bio-inspired flying robot sheds light on insect piloting  
550 abilities. *Current Biology.* 17, 329-335.

551 Franceschini, N., Ruffier, F., Serres, J., and Viollet, S. (2009). Optic flow based visual guidance: from  
552 flying insects to miniature aerial vehicles. In *Aerial Vehicles*, T.M. Lam, ed. (In-Tech), pp. 747-770.

553 von Frisch, K. (1948). Gelöste und ungelöste Rätsel der Bienensprache. *Naturwissenschaften.* 35, 38-43.

554 Gibson, J.J. (1950). *The perception of the visual world.* (Boston: Houghton Mifflin).

555 Horridge, G.A. (1987). The evolution of visual processing and the construction of seeing system. *Proc.*  
556 *Roy. Soc. Lond. B.* 230, 279-292.

557 Humbert, J.S., Hyslop, A., and Chinn, M. (2007). Experimental validation of wide-field integration meth-  
558 ods for autonomous navigation. *Proc. IEEE int. conf. intelligent robots and systems.*

559 Ibbotson, M.R. (2001). Evidence for velocity-tuned motion-sensitive descending neurons in the honeybee.  
560 *Proc. Roy. Soc. Lond. B.* 268, 2195-2201.

561 Lewis, M.A. (1997). *Visual Navigation in a Robot using Zig-Zag Behavior*, NIPS.

562 Nachtigall, W., Widmann, R., and Renner, M. (1971). Über den ortsfesten freien Flug von Bienen in  
563 einem Saugkanal. *Apidologie.* 2, 271-282.

564 Netter, T., and Franceschini, N. (2002). A robotic aircraft that follows terrain using a neuromorphic eye.  
565 *Proc. IEEE int. conf. intelligent robots and systems.* 129-134.

566 Neumann, T.R., and Bühlhoff, H.H. (2001). Insect visual control of translatory flight. *LNCS/LNAI.* 2159,  
567 627-636.

568 Pichon, J.M., Blanes, C., and Franceschini, N. (1989). Visual guidance of a mobile robot equipped with a  
569 network of self-motion sensors. *Proc. SPIE* 1195, 44-53.

570 Preiss, R. (1987). Motion parallax and figural properties of depth control flight speed in an insect. *Biol.*  
571 *Cyb.* 57, 1-9.

572 Pudas, M., et al. (2007). A miniature bio-inspired optic flow sensor based on low temperature co-fired  
573 ceramics (LTCC) technology. *Sensors and Actuators A.* 133, 88-95.

574 Riley, J.R., et al. (2003). The Automatic Pilot of Honeybees. *Proc. Roy. Soc. Lond.* 270, 2421-2414.

575 Ruffier, F., and Franceschini, N. (2003). Bio-inspired optical flow circuits for the visual guidance of micro-  
576 air vehicles. *IEEE int. symp. circuits and systems.* 3, 846-849.

577 Ruffier, F., and Franceschini, N. (2005). Optic flow regulation: the key to aircraft automatic guidance.  
578 *Robotics and Autonomous Systems.* 50(4), 177-194.

579 Sane, S.P., and Dickinson, M.H. (2002). The aerodynamic effects of wing rotation and a revised quasi-  
580 steady model of flapping flight. *J. Exp. Biol.* 205, 1087-1096.

581 Santos-Victor, J., Sandini, G., Curotto, F., and Garibaldi, S. (1995). Divergent stereo in autonomous  
582 navigation: from bees to robots. *Int. J. of Comp. Vision.* 14, 159-177.

583 Schilstra, C., and van Hateren, J.H. (1999). Blowfly flight and optic flow. I. Thorax kinematics and flight  
584 dynamics. *J. Exp. Biol.* 202, 1481-1490.

585 Seidl, R., and Kaiser, W. (1981). Visual field size, binocular domain and the ommatidial array of the  
586 compound eyes in worker honey bees. *J. Comp. Physiol. A* 143, 1726.

587 Serres, J., Dray, D., Ruffier, F., and Franceschini, N. (2008). A vision-based autopilot for a miniature  
588 air-vehicle: joint speed control and lateral obstacle avoidance. *Autonomous Robot.* 25, 103 -122.

589 Serres, J., Ruffier, F., Masson, G.P., and Franceschini, N. (2008). A bee in the corridor: centering and  
590 wall-following. *Naturwissenschaften.* 95, 1181-1187.

591 Srinivasan, M.V., Lehrer, M., Kirchner, W.H., and Zhang, S.W. (1991). Range perception through appar-  
592 ent image speed in freely flying honeybees. *Vis. Neurosci.* 6, 519-535.

593 Srinivasan, M.V., Zhang, S.W., Lehrer, M., and Collett, T.S. (1996). Honeybee navigation en route to the  
594 goal: visual flight control and odometry. *J. Exp. Biol.* 199, 237-2446.

595 Srinivasan, M.V., Zhang, S.W., Chahl, J.S., Barth, E., and Venkatesh, S. (2000). How honeybees make  
596 grazing landings on flat surfaces. *Biol. Cyb.* 83, 171-183.

- 597 Tammero, L.F., and Dickinson, M.H. (2002). Collision-avoidance and landing responses are mediated by  
598 separate pathways in the fruit fly, *Drosophila melanogaster*. *J. Exp. Biol.* 205, 2785-2798.
- 599 Vickers, N.J, and Baker, T.C. (1994). Visual feedback in the control of pheromone-mediated flight in  
600 *Heliothis virescens* males (Lepidoptera: noctuidae). *J. Insect Behav.* 7, 605-631.
- 601 Wakakuwa, M., Kurasawa, M., Giurfa, M., and Arikawa, K. (2005). Spectral heterogeneity of honeybee  
602 ommatidia. *Naturw.* 92, 464-467.
- 603 Weber, K., Venkatesh, S., and Srinivasan, M.V. (1997). Insect inspired behaviours for the autonomous  
604 control of mobile robots, M.V. Srinivasan and S. Venkatesh, Eds. *From living eyes to seeing machines.*  
605 (Oxford: Oxford University Press).
- 606 Zeil, J., Boeddeker, N., and Hemmi, J.M. (2008) Visually guided behavior. In *New Encyclopedia of Neu-*  
607 *roscience* (Amsterdam: Elsevier Science Publishers), in press, 2008.
- 608 Zufferey, J.-C., and Floreano, D. (2005). Toward 30-gram autonomous indoor aircraft: vision-based obsta-  
609 cle avoidance and altitude control. *Proc. IEEE Int. Conf. on Robotics and Automation.* pp. 2594-2599,  
610 Barcelona, Spain.

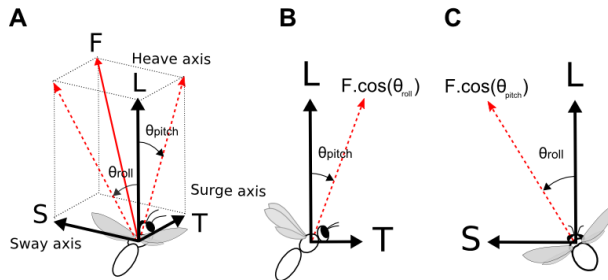


Figure 1: (A) Resolution of the mean flight-force vector  $\vec{F}$  along the surge X-axis giving the forward thrust  $T$ , along the sway Y-axis giving the side thrust  $S$ , and along the heave Z-axis giving the vertical lift  $L$ . (B) Pitching the mean flight-force vector  $\vec{F}$  by an angle  $\theta_{pitch}$  generates a forward thrust  $T$ . (C) Rolling the mean flight-force vector  $\vec{F}$  by an angle  $\theta_{roll}$  generates a side thrust  $S$ .

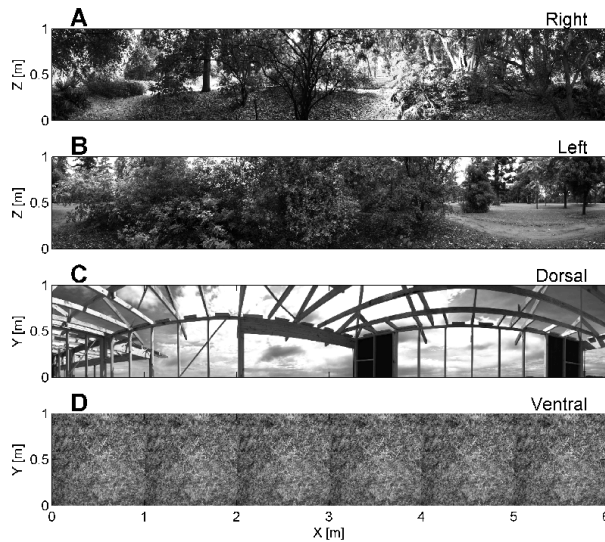


Figure 2: The grayscale natural scenes used to line the 4 internal faces of the simulated tunnel. Resolution of the images was  $1000 \times 6000$  pixels ( $1 \text{ pixel} = 1 \text{ mm}^2$ ). Images are therefore  $1 \times 6$ -meter in size. All four faces of the tunnel were lined with different images: right wall (A), left wall (B), roof (C), and ground (D).

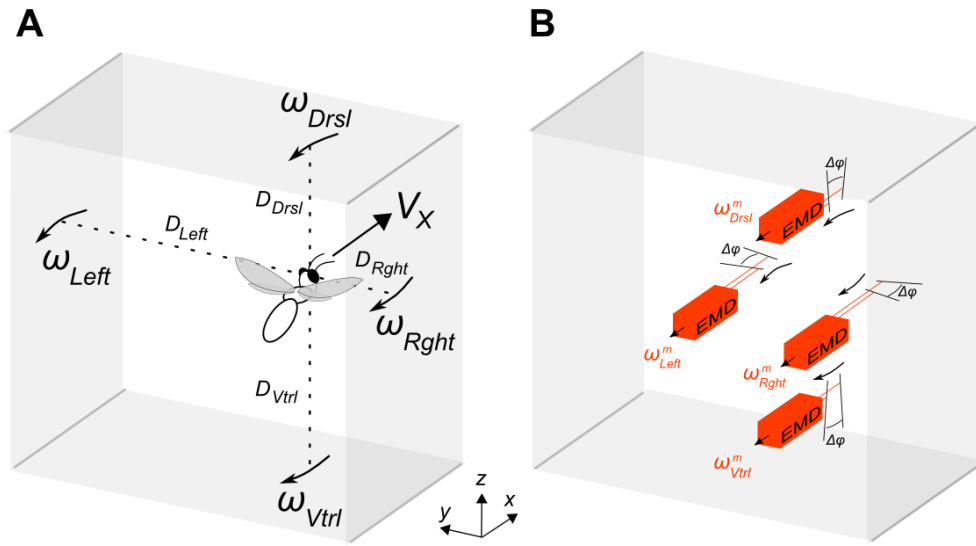


Figure 3: (A) A simulated bee flying at forward speed  $V_x$  along a tunnel generates an OF (Eq. 8) that depends on the perpendicular distance (right  $D_{Right}$ , left  $D_{Left}$ , ventral  $D_{Vtrl}$ , dorsal  $D_{Drsl}$ ) from the tunnel surfaces. The simulated bee is equipped with four OF sensors. The sensors' axes are always oriented at fixed roll and pitch orientations, perpendicular to the walls, ground and roof, respectively, and the OF is generated laterally ( $\omega_{Left}$  and  $\omega_{Right}$ ), ventrally ( $\omega_{Vtrl}$ ) and dorsally ( $\omega_{Drsl}$ ). (B) Each OF sensor consists of only two photoreceptors (two pixels) driving an Elementary Motion Detector (EMD). The visual axes of the two photoreceptors are separated by an interreceptor angle  $\Delta\phi = 4$  deg.



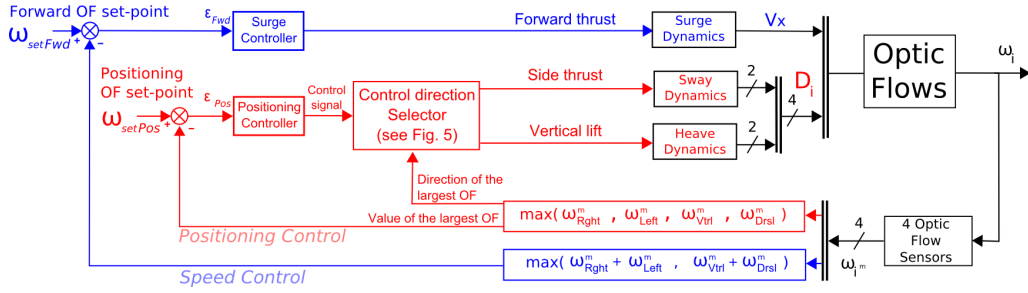


Figure 4: The ALIS autopilot is based on two interdependent visual feedback loops, each with its own OF set-point: a *speed control* loop (in blue) and a *positioning control* loop (in red). The surge controller adjusts the pitch angle  $\theta_{pitch}$  (that determines  $V_x$  via the bees' surge dynamics) on the basis of whichever sum of the two coplanar (horizontal or vertical) OFs measured is the largest. This value is compared with the forward OF set-point  $\omega_{setFwd}$ . The surge controller commands the forward speed so as to minimize the error  $\epsilon_{Fwd}$ . The positioning controller controls the roll angle  $\theta_{roll}$  (or the stroke amplitude  $\Delta\Phi$ ), which determines the distances to the walls (or the distances to the ground and to the roof), depending on the sway (or heave) dynamics on the basis of whichever of the four measured OFs is the largest. The latter value is compared with the positioning OF set-point  $\omega_{setPos}$ . At any time, the direction of avoidance is given by a *Control direction Selector* that multiplies the control signal by a *direction factor* depending on the *direction of the maximum OF* signal (see Fig. 5). The positioning controller (Proportional-Derivative, PD) commands the sway (or heave) dynamics so as to minimize the error  $\epsilon_{Pos}$ . The dash across the connection lines indicates the number of variables involved.  $D_i$  is the distance to the surface involved (see Eq. 7).

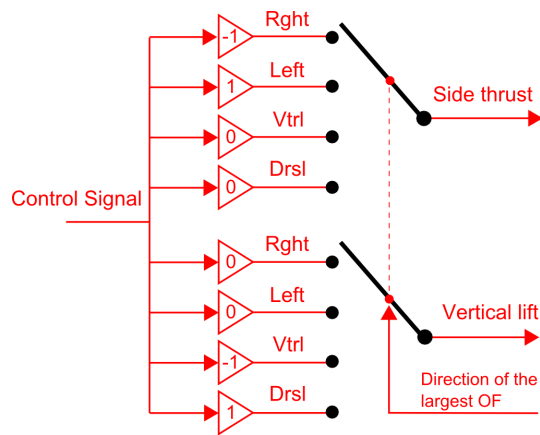


Figure 5: The *Control direction Selector* automatically selects the tunnel surface to be followed (wall, ground or roof) by multiplying the control signal (the output from the *Positioning controller*) by a *direction factor* that depends on the *direction of the largest OF* signal. Note that the sway and heave dynamics can be driven alternately, depending on which OF (side or vertical) is the largest at any given time. The input to the sway or heave dynamics that is not relevant is set to zero. In the example shown here, the direction of the maximum OF is “right”. Consequently, the output for the Side thrust is the control signal multiplied by -1 and the output for the Vertical thrust is the control signal multiplied by 0.

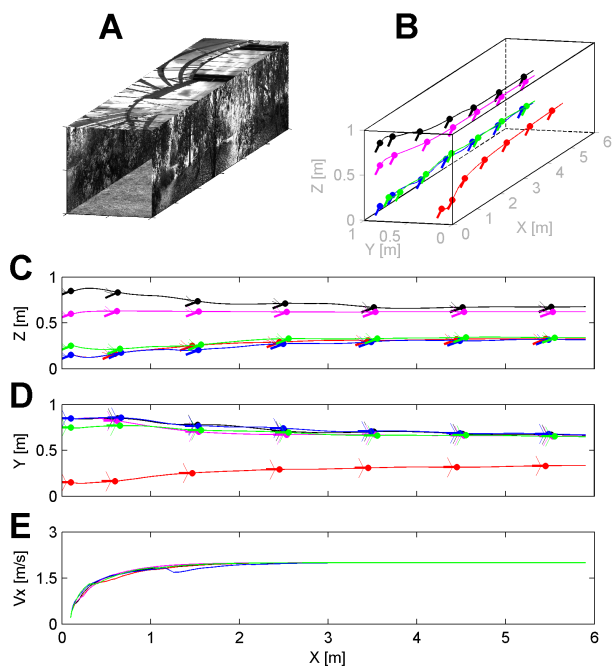


Figure 6: (A) Perspective view of the straight flight tunnel. (B) Simulated bee's 3-D trajectory starting at  $x_0 = 0.1$  m, with initial speed  $V_{x0} = 0.2$  m/sec, and various  $y_0$  and  $z_0$ , plotted every 500 msec. (C) Trajectory in the vertical plane ( $x, z$ ), every 500 msec. (D) Flight track in the horizontal plane ( $x, y$ ), plotted every 500 msec. (E) Forward speed  $V_x$  profile.

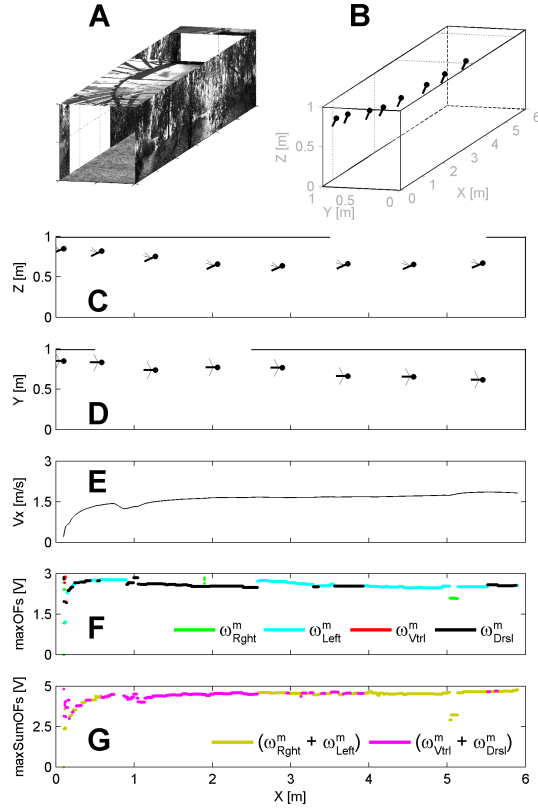


Figure 7: (A) Perspective view of the straight flight tunnel including two "no contrast" zones. (B) Simulated bee's 3-D trajectory starting at  $x_0 = 0.1$  m,  $y_0 = 0.85$  m,  $z_0 = 0.85$  m, at the forward speed  $V_{x.o} = 0.2$  m/sec, plotted every 500 msec. (C) Trajectory in the vertical plane (x, z), every 500 msec. (D) Trajectory in the horizontal plane (x, y), plotted every 500 msec. (E) Forward speed  $V_x$  profile. (F) Positioning feedback signal determined by the largest output from the four OF sensors (right OF sensor = green; left OF sensor = cyan; ventral OF sensor = red; dorsal OF sensor = black). (G) Forward feedback signal determined by the largest sum of the two diametrically opposed OF sensors (horizontal OF sensors = yellow; vertical OF sensors = magenta).

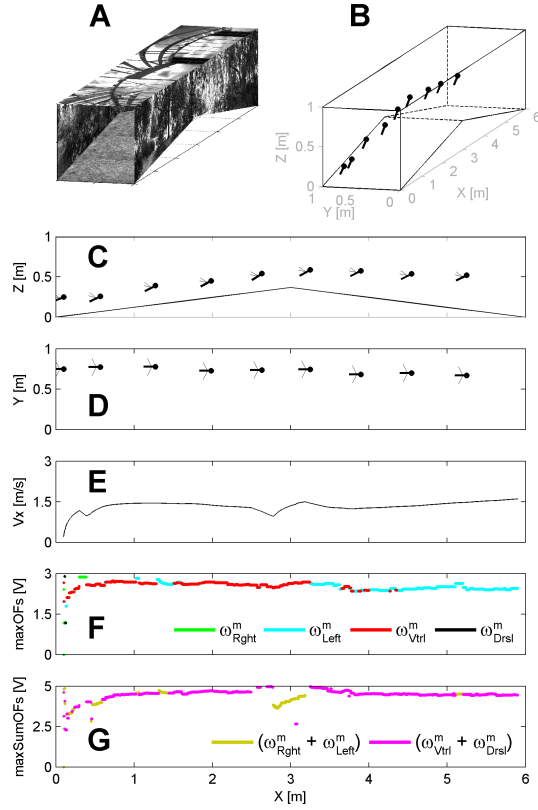


Figure 8: (A) Perspective view of the tapered tunnel. (B) Simulated bee's 3-D trajectory starting at the initial coordinates  $x_0 = 0.1$  m,  $y_0 = 0.75$  m,  $z_0 = 0.25$  m, and at the speed  $V_{x_0} = 0.2$  m/sec, plotted every 500 msec. (C) Trajectory in the vertical plane (x, z), every 500 msec. (D) Trajectory in the horizontal plane (x, y), plotted every 500 msec. (E) Forward speed  $V_x$  profile. (F) Positioning feedback signal determined by the largest output from the four OF sensors (right OF sensor = green; left OF sensor = cyan; ventral OF sensor = red; dorsal OF sensor = black). (G) Forward feedback signal determined by the largest sum of the two diametrically opposed OF sensors (horizontal OF sensors = yellow; vertical OF sensors = magenta).

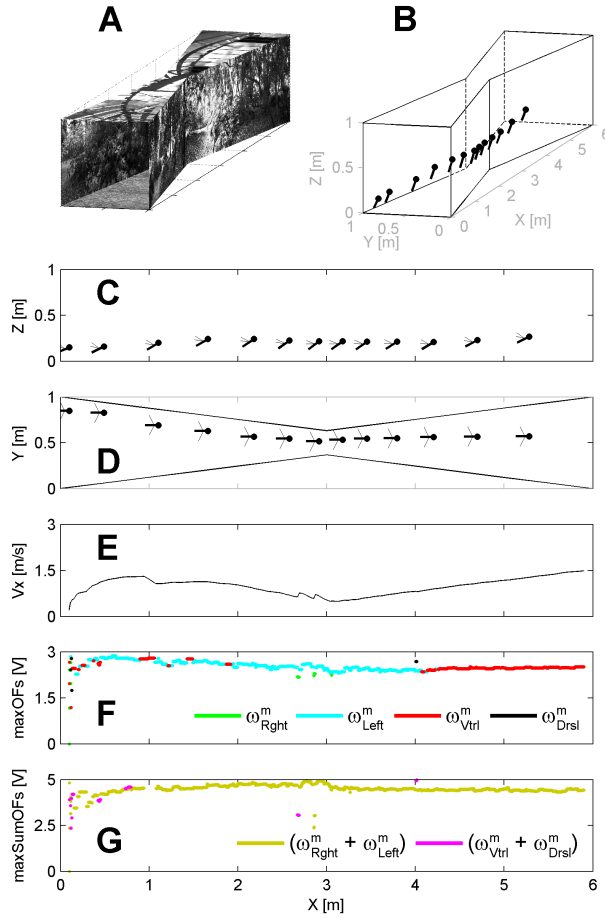


Figure 9: (A) Perspective view of the tapered tunnel. (B) Simulated bee's 3-D trajectory starting at the initial coordinates  $x_0 = 0.1$  m,  $y_0 = 0.85$  m,  $z_0 = 0.15$  m, and at the speed  $V_{x_0} = 0.2$  m/sec, plotted every 500 msec. (C) Trajectory in the vertical plane ( $x, z$ ), every 500 msec. (D) Trajectory in the horizontal plane ( $x, y$ ), plotted every 500 msec. (E) Forward speed  $V_x$  profile. (F) Positioning feedback signal determined by the largest output from the four OF sensors (right OF sensor = green; left OF sensor = cyan; ventral OF sensor = red; dorsal OF sensor = black). (G) Forward feedback signal determined by the largest sum of the two diametrically opposed OF sensors (horizontal OF sensors = yellow; vertical OF sensors = magenta).

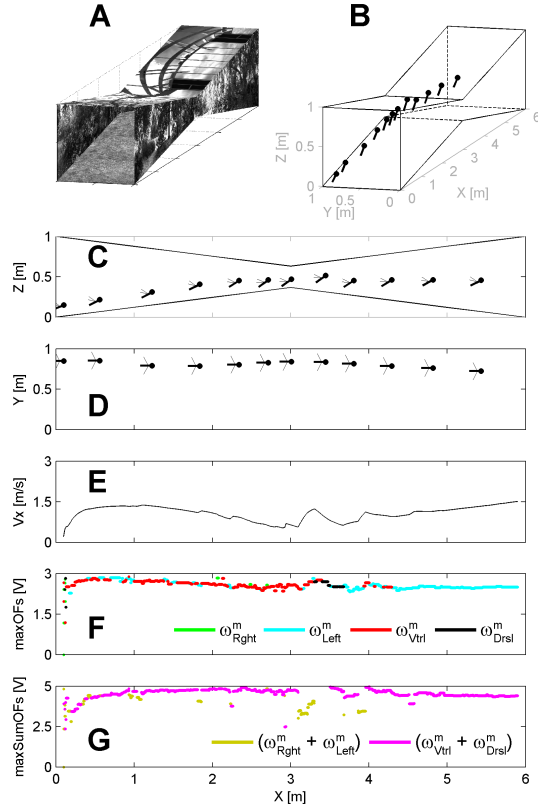


Figure 10: (A) Perspective view of the tapered tunnel. (B) Simulated bee's 3-D trajectory starting at the initial coordinates  $x_0 = 0.1$  m,  $y_0 = 0.85$  m,  $z_0 = 0.15$  m, and at the speed  $V_{x_0} = 0.2$  m/sec, plotted every 500 msec. (C) Trajectory in the vertical plane ( $x, z$ ), every 500 msec. (D) Trajectory in the horizontal plane ( $x, y$ ), plotted every 500 msec. (E) Forward speed  $V_x$  profile. (F) Positioning feedback signal determined by the largest output from the four OF sensors (right OF sensor = green; left OF sensor = cyan; ventral OF sensor = red; dorsal OF sensor = black). (G) Forward feedback signal determined by the largest sum of the two diametrically opposed OF sensors (horizontal OF sensors = yellow; vertical OF sensors = magenta).

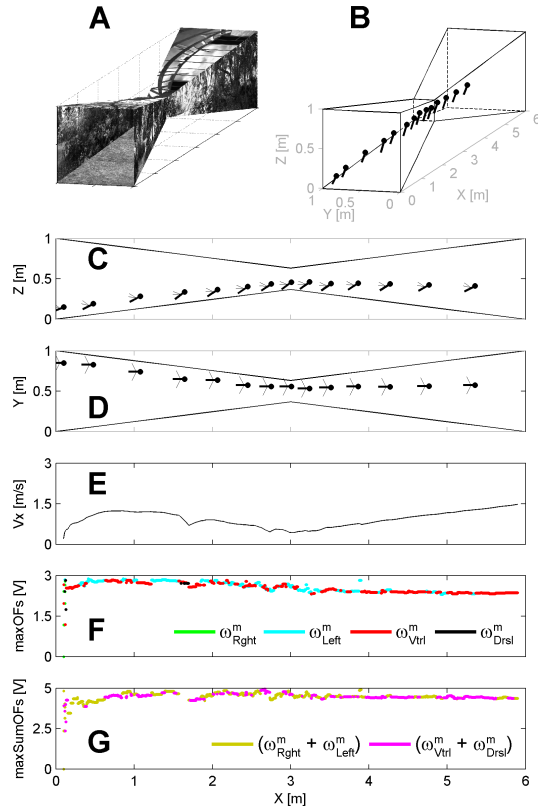


Figure 11: (A) Perspective view of the tapered tunnel. (B) Simulated bee's 3-D trajectory starting at initial coordinates  $x_0 = 0.1$  m,  $y_0 = 0.85$  m,  $z_0 = 0.15$  m, and at the speed  $V_{x_0} = 0.2$  m/sec, plotted every 500 msec. (C) Trajectory in the vertical plane ( $x, z$ ), every 500 msec. (D) Trajectory in the horizontal plane ( $x, y$ ), plotted every 500 msec. (E) Forward speed  $V_x$  profile. (F) Positioning feedback signal determined by the largest output from the four OF sensors (right OF sensor = green; left OF sensor = cyan; ventral OF sensor = red; dorsal OF sensor = black). (G) Forward feedback signal determined by the largest sum of the two diametrically opposed OF sensors (horizontal OF sensors = yellow; vertical OF sensors = magenta).